

High-efficiency TOPCon solar cell with superior P + and P++ layer via one-step processing

Xin Liu^a, Jianxin Sun^a, Yixuan Huang^a, Longqing Jiang^a, Shuangyu Liu^a, Feng Qian^b, Honglie Shen^b, Yang Yang^c, Rulong Chen^c, Guanghua Song^d, Juan Hong^{a,b,*}

^a College of Mechanical Engineering, Yancheng Institute of Technology, Yancheng, Jiangsu 224051, China

^b College of Materials Science and Technology, Nanjing University of Aeronautics and Astronautics, Nanjing 210016, China

^c Jiangsu Runergy Yueda PV Technology Co., Ltd, Yancheng, Jiangsu 224000, China

^d Popsolar Technology Co., Ltd, Taixin, Jiangsu 225400, China



ARTICLE INFO

Keywords:

Molecular dynamics
Boron doping
Boron-doped Si paste
Selective emitter
TOPCon solar cells

ABSTRACT

The boron diffusion process in the front field of N-type tunnel oxide passivated contact (TOPCon) solar cells is crucial for PN junction formation and the creation of a selective emitter. This study presents a theoretical model of boron diffusion in silicon using molecular dynamics. The research examines the mean square displacement and diffusion coefficient of boron atoms at varying temperatures, confirming their diffusion behavior. The simulations indicate predominant boron diffusion in the z-direction within the silicon matrix, with the diffusion depth being temperature dependent. The optimal temperature range for boron diffusion in silicon is identified as 950 °C to 1050 °C. Using boron-doped silicon paste and boron trichloride as dopants, thermal diffusion experiments were conducted to fabricate the front-field PN junction (p^+ layer) and selective emitter (p^{++} layer) by one step. Subsequent processing and performance evaluation were performed on a production line. Experimental findings reveal a decrease in boron diffusion at higher temperatures, reduced sheet resistance, increased doping concentration, and deeper junction formation. The ideal boron concentration in the p^+ layer is 8.68×10^{18} atom/cm³ with a depth of 0.53 μm, while the p^{++} layer is 2.35×10^{19} atom/cm³ and 0.82 μm. The efficiency of the optimized TOPCon + cell production line reaches up to 25.17 %, marking an improvement of 0.23 % over the standard cell production line. This research contributes to elucidating the mechanism of boron diffusion and offers insights for enhancing the efficiency of TOPCon solar cells.

1. Introduction

In recent years, tunnel oxide passivation contact (TOPCon) solar cells have attracted significant attention among researchers due to their notable efficacy in solar energy conversion [1–5]. The diffusion of boron (B) on the front surface of n-type TOPCon cells plays a pivotal role in establishing PN junctions, resulting in the formation of a lightly doped p^+ layer [6–8]. The concentration and depth of this diffusion layer have a direct effect on the generation and recombination of photogenerated carriers [9,10]. Concurrently, localized diffusion of high-concentration B elements beneath the printed metal electrode region leads to the creation of a selective emitter(SE), forming a heavily doped p^{++} layer. This, in turn, enhances the contact between the silicon (Si) substrate and the metal electrode, thereby facilitating the carrier output [10]. The selection of diffusion concentration and depth for both the p^+ and p^{++}

layers significantly influences the electrical parameters of the TOPCon cell [11]. Consequently, it becomes crucial to conduct an in-depth analysis of the B diffusion mechanism, optimize the diffusion process, and attain the appropriate diffusion characteristics for the p^+ and p^{++} layers [11,12]. These steps are primary for further enhancing the photovoltaic conversion efficiency of solar cells.

Currently, the body of theoretical research on B diffusion, especially at the atomic scale, remains relatively limited. Babak Sadigh *et al.* [13] determined the diffusion path of B in Si based on first-principles density functional theory (DFT) energies obtained through local-density approximation (LDA) and generalized gradient approximation(GGA). However, their study did not investigate the specific effects of the doping process on B diffusion. Kurachi *et al.* [14] established a physical diffusion model for the thermal diffusion of borosilicate glass films (BSG), albeit limited in its ability to visually observe atomic-level

* Corresponding author at: Hope Avenue Road 1, 224051, Yancheng, Jiangsu Province, China.

E-mail address: jameshong@ycit.cn (J. Hong).

diffusion phenomena. Molecular dynamics, on the other hand, provides a more intuitive portrayal of the complex mechanism and patterns of B atom migration [15], which can predict B atom diffusion characteristics at the atomic scale. Therefore, molecular dynamics methods enables a deeper and more accurate understanding of the B atom diffusion mechanism.

In contrast, there is an abundance of reports pertaining to the experimental investigation of B diffusion. Researchers have systematically explored the mechanisms and applications of B diffusion through process optimization, analysis of influencing factors, investigation of diffusion kinetics, and implementation of surface protection measures. For instance, Wang *et al.* [16] achieved precise control over the rate and profile of B diffusion by altering key process parameters in B trichloride tube furnace diffusion, including driving temperature, oxidation temperature, and B trichloride gas flow. Consequently, they obtained peak concentrations of the prepared p^{++} and p^+ layers, measuring 3.3×10^{19} atoms/cm³ and 6.6×10^{18} atoms/cm³, respectively. This effectively mitigated the electron concentration at the effective surface, thereby reducing recombination. Cheng *et al.* [17] deposited a PECVD B-doped a-SiOx: H layer onto an n-type c-Si wafer as a doping source. Subsequently, through the optimization of PECVD deposition and subsequent annealing/etching processes, they achieved a B diffusion zone with sheet resistance ranging from 60 to 100 Ω/\square and a junction depth of 1.2–1.5 μm . While the aforementioned research methodologies have yielded specific results in B diffusion experiments, they fall short in elucidating the underlying mechanisms of B diffusion. To comprehensively understand B diffusion, it is crucial to combine experimental data with simulation. Furthermore, the present methodology for fabricating the p^+ and p^{++} layers is intricate, necessitating multiple B diffusion steps in both laser doping and two-step diffusion techniques, which greatly increases cost. Therefore, Li *et al.* [18] introduced the concept of the B SE structure through one-step diffusion method using masks and etching. By employing the optimized B SE, they determined the appropriate sheet resistance for the p^+ layer and the optimal range for the junction depth of the p^{++} layer. Nevertheless, this technique is constrained by its intricate technological demands, exacting precision prerequisites, and substantial costs, thereby impeding its widespread implementation within the industrial sphere.

In this paper, We initially simulate the diffusion process of B atoms within Si wafers at various temperatures and durations using the molecular dynamics method. Through simulation, we scrutinize the diffusion behavior and thermal diffusion patterns of B atoms, ultimately calculating the diffusion coefficient of B in Si. Subsequently, a new method for preparing PN junction and SE are proposed. The traditional B trichloride and B-doped Si paste were used as doping sources to conduct B diffusion experiments, and then p^+ and p^{++} layers were formed in a tube diffusion furnace by one step. The method has low cost and simple operation, can simplify the B diffusion process, and can expand the gap of doping amount between p^+ and p^{++} layers. Then, the influence of time and temperature on the diffusion characteristics of B atoms was analyzed and an optimization experimental scheme was proposed. The appropriate sheet resistance in p^+ layer and the optimum range of the junction depth in p^{++} layer were determined. Using the optimized one-step B diffusion process, the batch efficiency of TOPCon + solar cells can achieve a gain of 0.1–0.3 %.

2. Molecular dynamics modeling

Molecular simulation [19–22] stands as a potent tool for scrutinizing the structural characteristics, properties, and physical-chemical interactions among nanoscale particles. In this study, molecular dynamics simulations were conducted utilizing the LAMMPS software package. The simulation employed the Tersoff [23] potential to depict the interactions among Si atoms, providing a commendable balance of performance and substantiated accuracy in simulating Si interactions. For the interactions involving B-Si and B-B, the nuclear force Yukawa [24]

potential was employed.

The initial configuration of the B-Si diffusion model comprised monocrystalline Si at the bottom and B-doped Si at the top. The monocrystalline Si was oriented along the (1,0,0) ideal plane, with a vacancy content of 0.01 %. To facilitate the study of B diffusion behavior, 10 % of Si atoms were randomly replaced by B atoms in the upper section of the model, creating the diffusion layer, while the Si substrate remained below it. Importantly, this simulation exclusively focuses on the diffusion of B atoms and does not consider the presence of other impurity elements. The simulation region dimensions were set at 61 Å × 61 Å × 88 Å, accommodating a total of 9417 atoms. Periodic boundary conditions were enforced in the transverse (X and Y) directions, effectively emulating an infinite planar Si crystalline. Additionally, the bottom of the monocrystalline Si and the top of the B-Si mixture (1.6 Å thickness) were held fixed along the vertical Z direction.

The simulation assumed that the initial atom velocities conformed to the Maxwell distribution, and the Velocity-Verlet algorithm was employed to calculate the Newton motion integral equation. To establish equilibrium with a constant number of atoms, pressure, and temperature (NVT), the Nose-Hoover thermostat was utilized, relaxing the system to 300 K over a duration of 10 ps. Subsequently, the temperature was rapidly increased to the preset value and maintained for 6 ns. Throughout the entire simulation, the external pressure remained at atmospheric levels, and a time step of 1 fs was employed. Notably, B atoms can only diffuse into Si at sufficiently high temperatures. Therefore, considering the experimental process parameters, temperatures of 750 °C, 850 °C, 950 °C, and 1050 °C were taken into consideration in this study. Snapshots from the LAMMPS simulations were visualized using Ovito. The diffusion snapshots at different temperatures after 6 ns relaxation are shown in Fig. 1 (To increase contrast, we zoom in or out on the size of the atoms).

3. Experimental section

3.1. B-doped Si paste preparation

In this study, the controlled doping of B into Si nanoparticles was achieved through a combination of the ball milling method and thermal annealing process [25,26]. BS20 [12] was synthesized using an optimized ball milling procedure, and subsequently, B-doped Si paste was successfully formulated using BS20 NPs and an organic carrier. Through

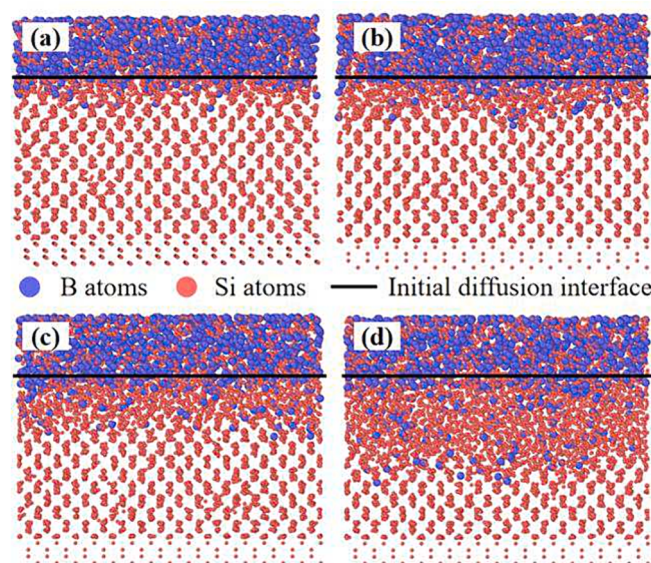


Fig. 1. Simulates 6 ns to obtain snapshots of B/Si at different temperatures. (a) 750 °C, (b) 850 °C, (c) 950 °C and (d) 1050 °C.

the process of screen printing and subsequent drying, a dense and uniform B-doped Si film was deposited onto the surface of a Si wafer, serving as a consistent B-doped surface source. The excellent printing characteristics of this film ensure uniform B-doping of Si wafers during the subsequent thermal diffusion process. A detailed account of the specific preparation process and process optimization can be found in prior work [12].

3.2. Thermal diffusion experiment and TOPCON cell preparation

The preparation of thermal diffusion experimental samples involved the use of Czochralski (Cz) n-type c-Si wafers with $\langle 100 \rangle$ orientation, measuring $182 \text{ mm} \times 182 \text{ mm} \times 0.16 \text{ mm}$ in size and possessing a resistivity in the range of $1\text{--}1.1 \Omega\cdot\text{cm}$, which were chosen for this study. Initially, a 25 wt% NaOH (Aladdin, 99.9 % metals basis) solvent was employed to eliminate saw damage and subjected to a 15 min treatment at 85°C . Subsequently, B-doped Si paste was screen-printed onto the c-Si wafer, utilizing two distinct screen printing patterns. One pattern comprised a $20 \text{ mm} \times 20 \text{ mm}$ square, with a thickness of $10 \mu\text{m}$ (EOM thickness), designed for assessing sheet resistance and doping performance. The other pattern took the form of a $30 \mu\text{m}$ wide, $10 \mu\text{m}$ thick (EOM thickness) line intended for creating deep p^{++}/n junctions in SE.

Following the screen printing process, the Si paste-coated Si wafers were dried at 230°C for 30 s. Subsequently, these Si wafers were spaced at approximately 15 mm intervals and subjected to annealing at temperatures of 750°C , 850°C , 950°C , and 1050°C , each for durations of 20 min, 40 min, and 60 min. The heating rate during annealing was maintained at $5^\circ\text{C}/\text{min}$ within a tubular furnace under a nitrogen atmosphere. After the diffusion process was completed, the BSG and Si paste were removed by $1\text{--}5 \text{ wt\% HF}$ (Amethyst 40 %, for analysis) and 15 wt\% KOH solvent, then the B-doping performance of p^+ and p^{++} layer were measured by ECV.

The fabrication of TOPCON cells was executed on a production line with a capacity of 15 MW, owned by Jiangsu Runyang Yueda Photovoltaic Technology Co., Ltd. The precise preparation procedure is as follows: the initial Si wafer treatment involved chemical cleaning and etching to eliminate surface contaminants and mechanical imperfections. Following cleaning, double-sided texturing was performed. Subsequently, the application of Si paste on the front surface of the Si wafer, following the metal electrode pattern, was carried out to create a paste-coated area. High-temperature thermal diffusion was employed to induce a reaction between the paste and the borosilicate glass within the paste-coated region. This led to the transformation of BSG into a B-Si mixture. The Si wafer, arranged in a back-to-back configuration, was then placed in a tube diffusion furnace for B diffusion. This process resulted in the formation of both shallow and heavily doped B zones, with BSG forming on the B expansion surface. The Si wafer underwent B diffusion within a high-temperature annealing (20 min at 950°C) furnace to establish the final PN junction, as depicted in Fig. 2. After removing the BSG layer from the back of the Si wafer using a chain

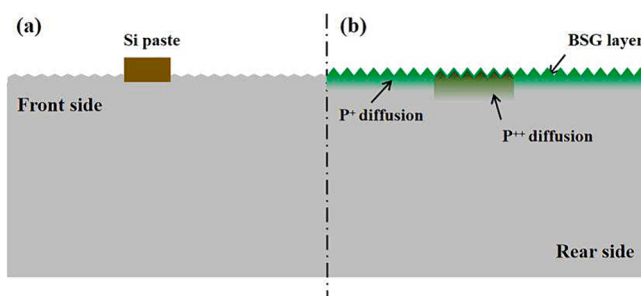


Fig. 2. Process scheme of one step for p^+ and p^{++} layer formation: (a) before diffusion: screen printing B-doped Si paste, (b) after diffusion: p^+/n and p^{++}/n junction formation.

hydrofluoric acid machine. Subsequently, the Si wafer was transferred to an alkaline polishing machine, the rear side undergoes alkaline etching using an 80°C KOH solution to achieve a reflectance of over 30 %.

Following the polishing step, the rear stack comprising SiO_x ($1.1\text{--}1.5 \text{ nm}$) and a-Si ($90 \pm 20 \text{ nm}$) was fabricated utilizing low pressure chemical vapor deposition (LPCVD) technology. Subsequently, the prepared sample underwent annealing in a tube furnace at 900°C for 45 min in the presence of a mixture of POCl_3 , O_2 , and N_2 to induce the crystallization of a-Si into poly-Si, while also doping it with phosphorus. During this process, the phosphorus within the deposited phosphorus-doped poly-Si layer formed covalent bonds with Si, providing electrons and creating a field passivation structure.

Subsequently, again cleaning the wafers and removing phosphosilicate glass (PSG) on the back and the BSG and Si paste on the front. Then the poly-Si wraparound side was etched in inline treatment with HF and batch-type treatment with a mixed solution of KOH and polishing additives. Passivation layers were deposited on the front and back surfaces. An aluminum oxide layer ($3 \text{ nm-}\text{AlO}_x$) was deposited on the front surface using ALD equipment for passivation, while a Si nitride layer ($82 \text{ nm-}\text{SiN}_x$) was deposited on the front surface using PECVD equipment for antireflection. A Si nitride passivation layer ($82 \text{ nm-}\text{SiN}_x$) was deposited on the back surface using PECVD. Electrodes were created by screen printing pastes onto the front and back surfaces. The front printed pattern of the wafer corresponds to the screen pattern of the applied Si paste, while the back adheres to the standard production line's pattern grid design. The front metal electrode with $15\text{--}25 \mu\text{m}$ width and $5\text{--}10 \mu\text{m}$ height was screen printed above the p^{++} layer, where the three dots with a diameter of $80 \mu\text{m}$ as mark points were used for alignment.

Finally, the Si wafer underwent optical injection processing and was subjected to testing. In comparison to the traditional TOPCon cell fabrication process, the key difference is that the B-diffusion step uses a one-step method to prepare the p^+/p^{++} layer, which is not present in the conventional Si wafer preparation process. A detailed overview of the preparation process is depicted in Fig. 3.

3.3. Test and analysis tools

The B doping curve was tested by the electrochemical capacitance–voltage (ECV) method. The electrical I-V performance of the cell was characterized by a Halm tester. The sheet resistance of the Si wafer is measured by the four-point probe method.

4. Results and discussion

4.1. Modeling results

4.1.1. Diffusion of B in Si at different temperatures

Fig. 4 and 5 depict the B atom diffusion process. As illustrated in Fig. 4, the position distribution of B atoms at various temperatures is shown, while Fig. 5 displays the position distribution of B atoms at different time intervals at 950°C . The quantity and depth of B atom diffusion are influenced not only by the diffusion temperature but also by the duration of diffusion. Higher temperatures and longer durations result in increased B atom diffusion from the source to the opposite side, leading to greater diffusion depth.

Specifically, at 750°C and 850°C , B atom diffusion is relatively insignificant, with only a minimal number of atoms diffusing along the z-axis direction. The number of diffused B atoms is small, and the diffusion depth is shallow at these lower temperatures. In contrast, as the temperature increases to 950°C and 1050°C , the depth of B atom diffusion significantly increases, and the quantity of diffused atoms substantially increases compared to that at lower temperatures.

In Fig. 5, it can be observed that after 200 ps of diffusion at 950°C , only a small quantity of B atoms diffused into the Si matrix. However, with increasing simulation time, both the number of diffused B atoms

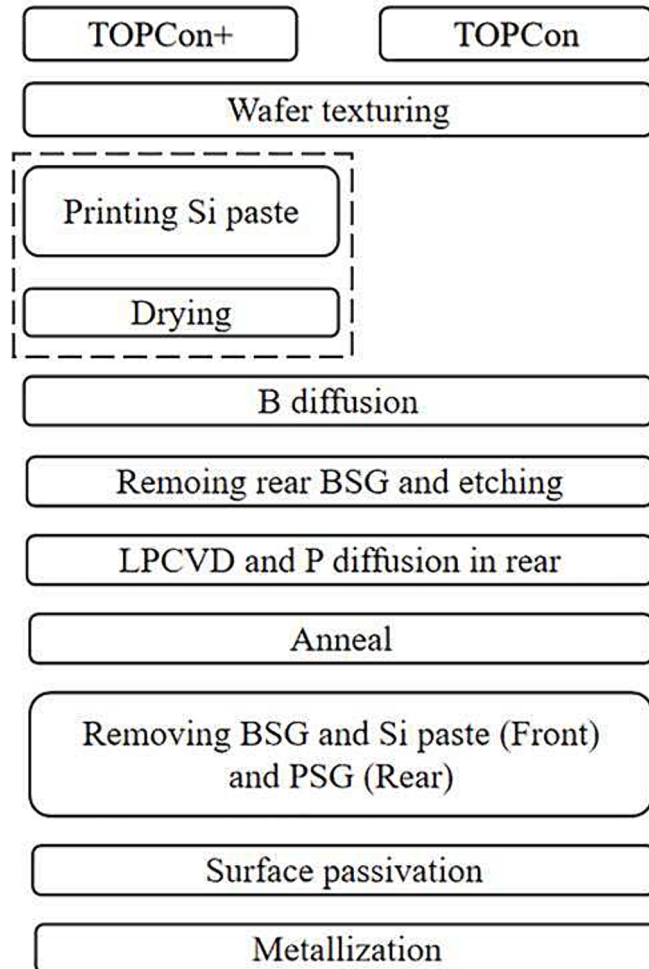


Fig. 3. Comparison of the TOPCon + and TOPCon battery preparation processes.

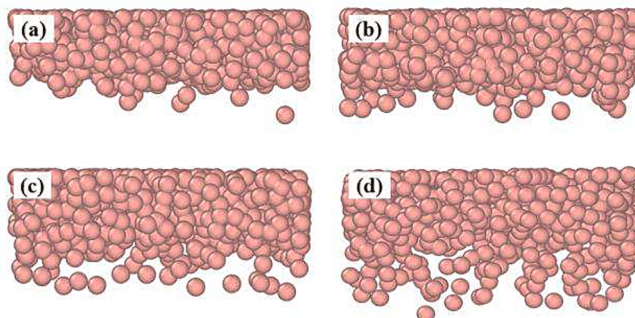


Fig. 4. Snapshot of B atom diffusion after 6 ns time at different temperatures. (a) 750 °C, (b) 850 °C, (c) 950 °C and (d) 1050 °C.

and the depth of diffusion progressively increase. Over an extended duration, such as 6 ns, the number and depth of B atom diffusion substantially increase. This behavior arises primarily due to the atomic characteristics of B, which has an atomic radius of 0.082 nm, while the Si atom possesses a radius of 0.118 nm, resulting in a mismatch ratio of 0.75. Consequently, lattice tension is generated during the diffusion process [27], leading to a slow diffusion rate and low solid solubility of B in Si. Hence, higher temperatures and longer durations are needed to facilitate effective diffusion. Typically, B diffusion behavior becomes prominent above 900 °C.

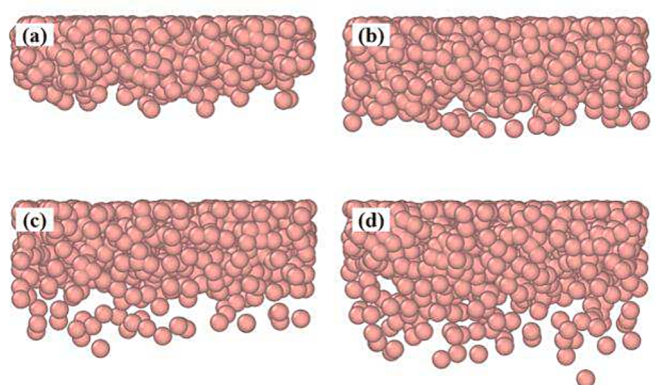


Fig. 5. Snapshots of B atom diffusion at different simulation times at 950 °C. (a) 200 ps, (b) 1 ns, (c) 3 ns and (d) 6 ns.

In Fig. 6, the concentration variations of B atoms in the z-direction following diffusion periods of 0 ns, 1 ns, 3 ns, and 6 ns at 950 °C are displayed. It is evident from the figure that the concentration of B atoms exhibits a consistent trend with time at each temperature: the concentration at the initial position (the B source region) diminishes over time, while the concentration at deeper levels (the doping region) increases with time. Moreover, at the same diffusion duration, higher temperatures result in lower surface B concentrations and deeper diffusion depths of B atoms. This observation signifies that B atoms continue to diffuse into the Si matrix over time, and higher temperatures lead to lower surface B concentrations and greater diffusion depths.

However, when temperatures reach 950 °C and 1050 °C, the difference in surface B atom concentrations becomes less pronounced. Nevertheless, the diffusion depth at 1050 °C surpasses that at 950 °C. This implies that when the B source concentration remains constant, there is a critical temperature threshold beyond which the number of B atoms in Si saturates, making it challenging for B atoms from the source to further diffuse into Si. At this point, B atoms within Si continue to penetrate deeper over time.

Additionally, the depth of B atom diffusion can be inferred from the concentration distribution, with the depth approximately determined based on the concentration range. As depicted in Fig. 7, at temperatures of 750 °C, 850 °C, 950 °C, and 1050 °C, the maximum diffusion depths are measured at 0.236 nm, 0.248 nm, 0.264 nm, and 0.346 nm, respectively. This result substantiates that the depth of the diffusion layer is influenced by both temperature and duration. Higher temperatures and longer diffusion times result in greater diffusion depths. In addition, it can be clearly seen from the figure that after the temperature reaches 950°C, the average diffusion depth increases significantly, and the maximum diffusion depth also increases significantly. This shows that 950°C is the turning point of B diffusion.

4.1.2. Diffusion coefficient

To prevent the nonphysical influence of ensemble pressure on the simulation box size, the entire system's dynamic calculation is conducted using the NVT ensemble. Following an initial relaxation period, the current coordinates of the B atom are recorded. Subsequent simulations involve periodic calculations of the mean square displacement (MSD) of the B atom in relation to these recorded coordinates. The MSD data collected during the sampling interval are used to generate a curve depicting how MSD changes over time. When this curve exhibits a linear increase, the diffusion coefficient of the B atom can be calculated utilizing the Einstein formula. MSD represents the mobility of particles, in-unit Å², and its calculation method is as follows:

$$MSD = \langle r^2(t) \rangle = \frac{1}{N} \sum_{i=1}^N (|r_i(t) - r_i(0)|^2) \quad (1)$$

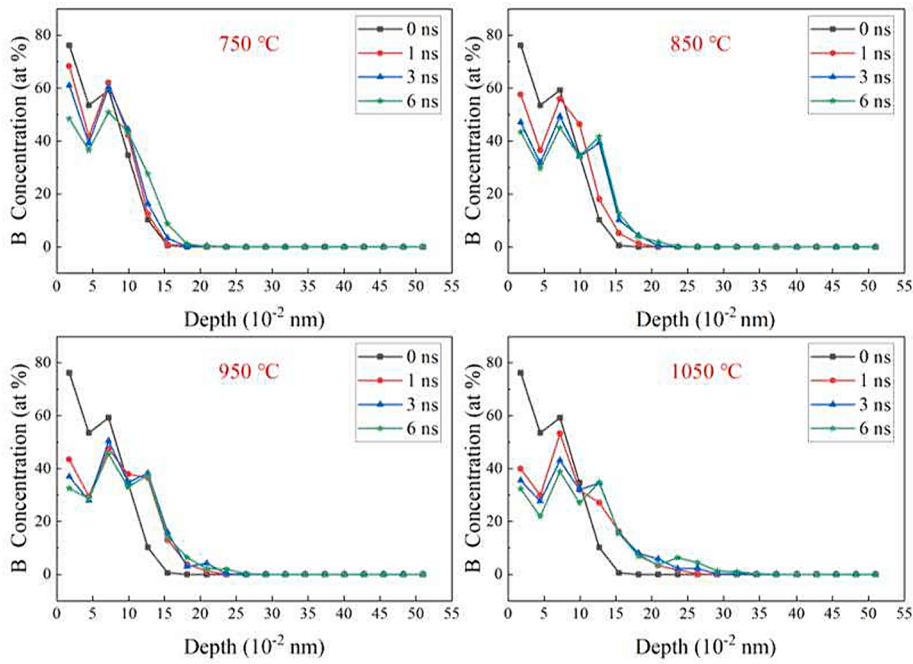


Fig. 6. The concentration distribution of B atoms along the Z direction at different temperatures and times.

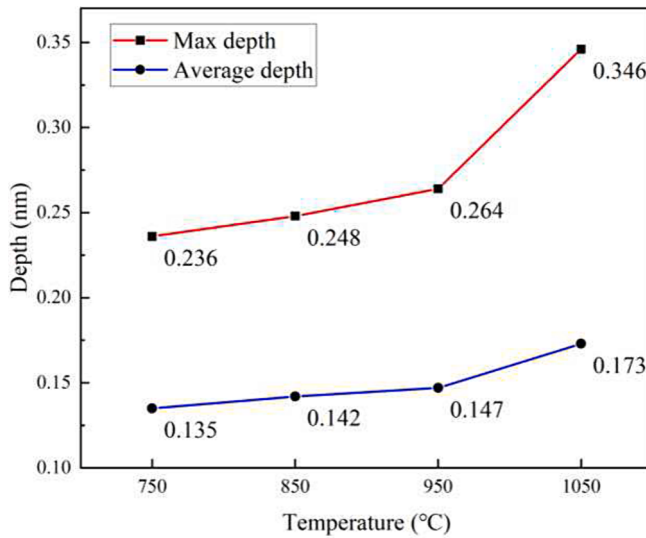


Fig. 7. The maximum diffusion depth and average diffusion depth of B atoms change with temperature within 6 ns.

where $\langle \rangle$ pairs should average all atoms in the group, and N corresponds to the number of atoms in the group.

In this study, based on the principles of the fluctuation-dissipation theory in statistical mechanics, two equivalent formulas can be employed to determine the diffusion coefficient (D) (m^2/s) in molecular dynamics simulation. The first method involves the Einstein relation, which is calculated using the MSD:

$$D = \lim_{t \rightarrow \infty} \frac{1}{6t} \langle |r_i(t) - r_i(0)|^2 \rangle = \frac{1}{6} d(\text{MSD}) \quad (2)$$

The other is the Green Kubo formula calculated by the velocity autocorrelation function.

$$D = \frac{1}{3} \int_0^\infty \langle v_i(t) \cdot v_i(0) \rangle dt \quad (3)$$

where $r_i(t)$, $r_i(0)$ and $v_i(t)$, $v_i(0)$ correspond to the displacement vector and velocity vector of the particle at time t and time 0, respectively.

The Green Kubo formula necessitates extensive statistical integration of the velocity autocorrelation function to derive the diffusion coefficient. In contrast, the Einstein formula directly relates to the MSD obtained from simulation results, offering a simpler and faster approach. To expedite data processing while ensuring the reliability of the calculated results, the diffusion coefficient of B atoms within the Si matrix was determined using the MSD method in this simulation.

According to Formula 1, the diffusion coefficient is essentially one-sixth of the slope of the MSD-t curve. Fig. 8 illustrates the relationship between the MSD of the system and time at various temperatures over a duration of 6 ns. These curves consistently exhibit a common trend: the MSD-t curve increases with both time and temperature. This observation underscores that higher temperatures lead to increased hopping frequencies of B atoms.

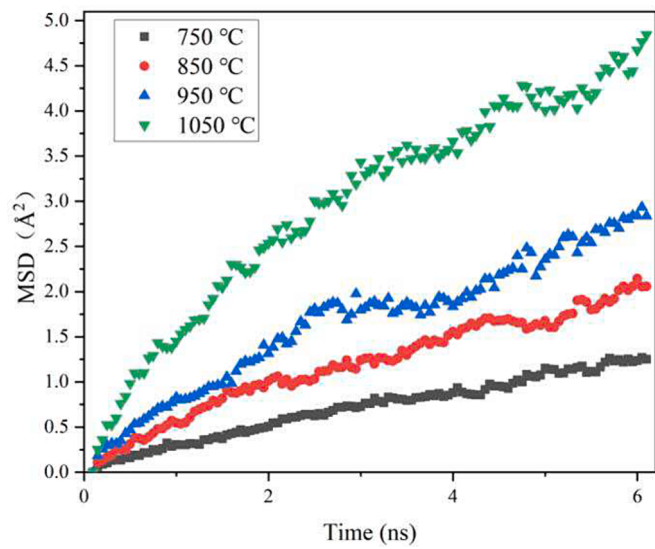


Fig. 8. Mean square displacement at different temperatures.

These MSD-t curves were subjected to linear fitting, and the corresponding diffusion coefficients were computed using Formulas 1 and 3. The relationship between the diffusion coefficient of B atoms and temperature is presented in Fig. 9. It is evident that within the simulation system, higher temperatures lead to larger diffusion coefficients for B atoms. The findings indicate that when the temperature reaches 950 °C, there is a substantial increase in the diffusion coefficient of B. Therefore, the appropriate temperature range for B diffusion should fall within 950–1050 °C. These simulation results align well with the experimental data, affirming their consistency with the expected trend.

The dominant axis of B atoms at temperatures of 750°C, 850°C, 950°C, and 1050°C is observed to be the Y-axis, Z-axis, Z-axis respectively, as depicted in Fig. S1. It is evident that the diffusion of B atoms primarily occurs along the Z-axis. The reason for not observing a predominant Z-direction diffusion at 750°C is attributed to the low temperature which results in a lower B diffusion coefficient. Consequently, it becomes challenging for B atoms to spread towards Si along the Z-axis. Most of the displacement of B atoms occurs only inside the B source, as shown in Fig. 1 (a). However, with the increase of temperature, the diffusion coefficient of B continues to increase, and B atoms continue to diffuse into Si along the z axis, as shown in Fig. 1 (b), (c) and (d).

The simulation results indicate: when the B source concentration in the Si paste remains constant, higher temperatures result in larger diffusion coefficients, leading to a greater influx of B atoms into the Si matrix and deeper diffusion depths, and the diffusion of Z-direction is dominant. However, when the temperature exceeds 950 °C, the average diffusion depth and the maximum diffusion depth suddenly increase. Therefore, the most favorable results are tentatively obtained in the temperature range of 950–1050 °C.

4.2. Experimental results

B powder [12] can also serve as a doping source for n-type Si. However, creating high concentrations (more than 10^{19} atom/cm³) of pure B doping sources with low oxygen content is challenging [28]. Moreover, when using a pure B source in high-temperature diffusion processes (above 1000 °C), the resulting B-doped layer tends to be nonuniform, adversely affecting the separation of photogenerated carriers. In the methodology employed in this study, B atoms are distributed in two primary forms. One part exists as Si-B-O bonds within the silica of BSG, while the other part is deposited on the surface of Si nanoparticles in the form of B-B and B-O bonds. During high-temperature doping, B atoms effectively diffuse, and during the thermal annealing process, B

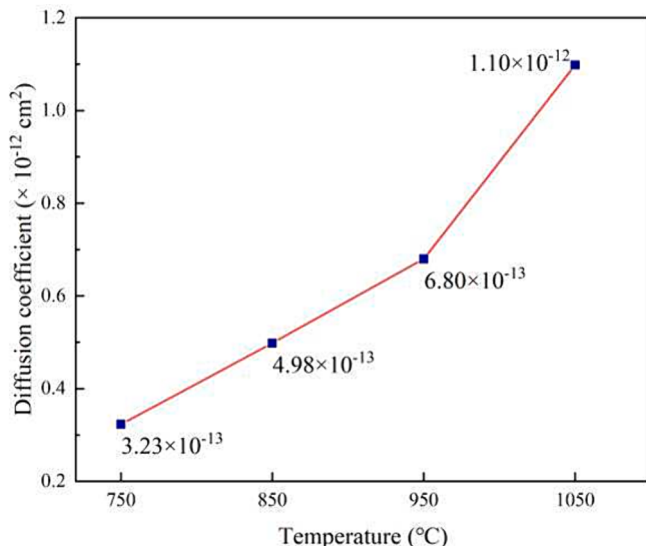


Fig. 9. The trend of the diffusion coefficient with increasing temperature.

atoms from both forms further penetrate into Si nanoparticles. This approach enhances the uniformity of the doping layer and significantly increases the doping rate of B atoms.

Fig. 10 (a) and (b) depict the schematic representation of the prepared Si paste and the schematic layout of the Si wafer used for the square resistance test after screen printing. The screen printing process of the Si paste is substantiated by results from the contour measurement image obtained via laser microscopy and the scanning electron microscope image, as presented in Fig. 10 (c) and (d). The square area's dimensions, as shown in Fig. 10 (b), measure approximately 20 mm × 20 mm. The boundary of this region is well defined, with no extensions. Following the preparation of the pretreated wafer, Si paste is screen-printed onto the front surface opening to create a densely packed linear Si paste area, as illustrated in Fig. 10 (c). The cross-section of the Si paste region is depicted in Fig. 10 (d). After drying for approximately 30 s at 250 °C, the dried Si paste attains a thickness of approximately 2 μm. Furthermore, the scanning electron microscope image reveals that the Si paste thickness exhibits excellent uniformity within the square area.

To determine the optimal diffusion time and temperature, the sheet resistance on the Si wafer was tested using the four-probe test method under various diffusion temperature and time conditions. This testing further confirms the B concentration on the Si wafer after thermal diffusion. Si wafers processed below 750 °C were not investigated since insufficient heat treatment does not effectively facilitate B atom diffusion.

As depicted in Fig. 11, the sheet resistance decreases as the thermal diffusion temperature and time increase. Specifically, at a given diffusion temperature, increasing the time results in a lower sheet resistance. Similarly, at a consistent diffusion time, elevating the temperature leads to decreased sheet resistance. This pattern indicates a gradual diffusion of B atoms into the Si wafer. At 850 °C, the sheet resistance decreases rapidly initially, but as time progresses, the surface source concentration diminishes, and the sheet resistance stabilizes until reaching 1050 °C. These findings align well with the simulation results presented in Fig. 6. As the temperature rises, the concentration of B atoms, or the doping concentration, increases, elevating the carrier concentration of the Si wafer and enhancing its conductivity, resulting in decreased sheet

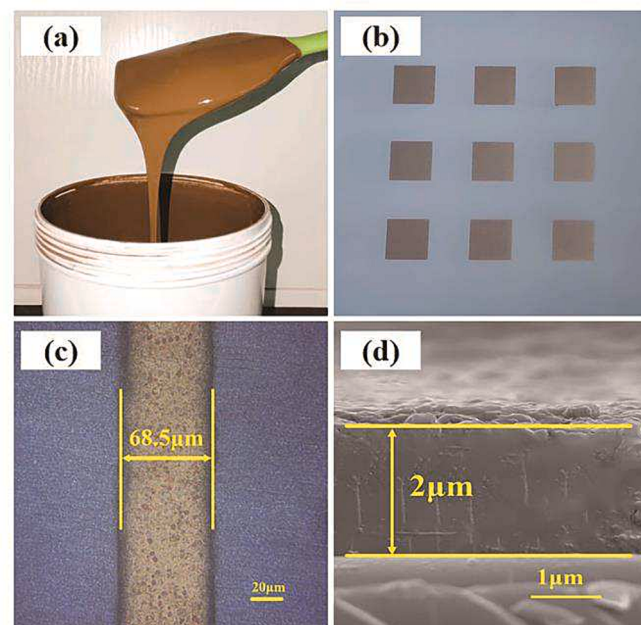


Fig. 10. The square area (b) formed and the linear region (c) by printing B-doped Si paste (a) on the Si wafer. (d) The cross section of the Si paste screen printed on the Si wafer.

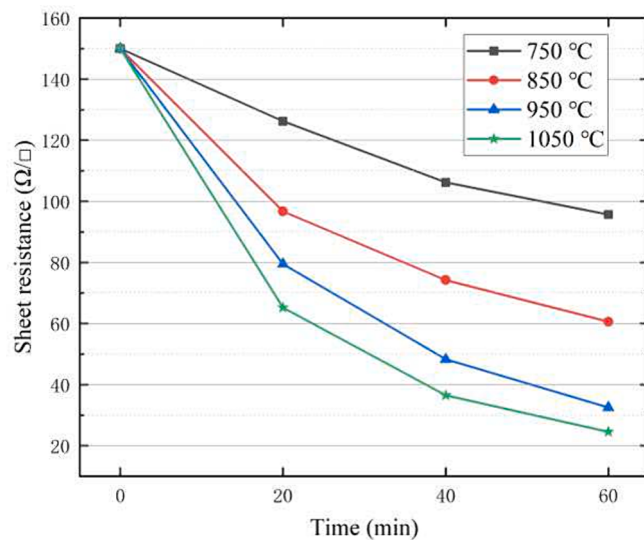


Fig. 11. Sheet resistance on Si substrate at different temperatures and different diffusion times.

resistance.

Fig. 12 displays the B doping curve of the Si wafer after thermal diffusion for 60 min at different temperatures, measured using the ECV. Higher temperatures correspond to higher B doping concentrations and deeper junction depths. In the junction depth range of 0.09–0.12 μm , the maximum doping concentrations at 750 °C, 850 °C, 950 °C, and 1050 °C are 8.23×10^{18} atom/cm³, 5.45×10^{19} atom/cm³, 4.32×10^{20} atom/cm³, and 9.17×10^{20} atom/cm³, respectively. The experimental results in terms of doping concentration closely mirror the trends observed in Fig. 6. Combining the simulation results and doping performance, the optimal conditions for preparing the p⁺⁺/n junction involve thermal diffusion at 950 °C for 20 min.

After the removal of the BSG layer, the relationship between the B concentration and the depth of the p⁺ layer and p⁺⁺ layer was estimated using ECV, as illustrated in Fig. 13. Within the junction depth range of 0.09–0.12 μm , the maximum doping concentrations for the p⁺ and p⁺⁺ layers are 8.68×10^{18} atom/cm³ and 2.35×10^{19} atom/cm³, respectively. The corresponding sheet resistances measure approximately 108.69 Ω/\square and 83.12 Ω/\square , respectively. The junction depths of the p⁺/n and p⁺⁺/n junctions are 0.53 μm and 0.82 μm , respectively. These results highlight that the use of B-doped Si paste, coupled with an appropriate thermal diffusion process, can significantly enhance the

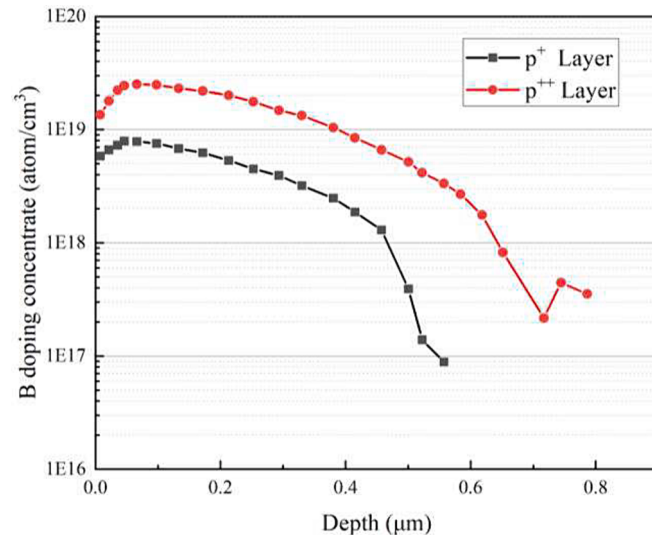


Fig. 13. The relationship between the B concentration measured by ECV and the depth of the p⁺ and p⁺⁺ layers at 950 °C.

performance of B doping.

The temperature and duration of B diffusion have a significant effect on the fill factor (FF) of the cell. Precisely controlling the temperature and duration of B diffusion can ensure that B diffuses to the appropriate depth on the cell's surface, thereby enhancing the FF [3,16,29,30]. Specifically, the temperature of B diffusion has an effect on the filling coefficient. Appropriate B diffusion temperature can promote the interfacial reaction between metal electrode and Si substrate, which contributes to the formation of low contact resistance. Secondly, the duration of B diffusion also affects the contact resistance between the metal electrode and the Si substrate. Appropriate B diffusion time can ensure that the interface between the metal electrode and the Si substrate forms a uniform and low contact resistance, which is conducive to the transport of electrons and the improvement of the filling coefficient.

Additionally, selecting the appropriate B doping concentration is crucial for improving the cell's FF. Excessive B doping concentration can result in an excessive surface dose and increased current loss in the cell. Conversely, a B doping concentration that is too low may not effectively enhance the FF. The high B surface doping concentration increases the contact resistance between the metal electrode and the Si substrate. In solar cells, the surface recombination rate refers to the speed of recombination of photogenerated carriers after reaching the surface. The higher surface recombination rate leads to an increase in the loss of photogenerated carriers. The increase of B doping concentration on the surface of the solar cell increases its recombination rate, resulting in more loss of photogenerated carriers when they reach the surface, thereby increasing the current loss in the solar cell. In addition, the high surface B doping concentration will also affect the electric field distribution on the surface of the solar cell, thus affecting the carrier transport and collection efficiency on these surfaces, resulting in an increase in current loss.

To further substantiate the benefits of this specific process condition (screen-printed Si paste and thermal diffusion at 950 °C for 20 min), a comparison was conducted between the I-V data of TOPCon + cells fabricated using this process and TOPCon cells produced via the standard production line procedure using the same batch of wafers. A summary of this comparative analysis is provided in Table 1. In general, TOPCon + cells with printed Si paste under appropriate thermal diffusion conditions exhibit higher efficiency than TOPCon cells without printed Si paste. This technology increases the efficiency of TOPCon cells on the normal production line by an average of approximately 0.12 % and up to 0.23 % in the most significant cases. A substantial portion of the improvement in cell efficiency can be attributed to a noteworthy

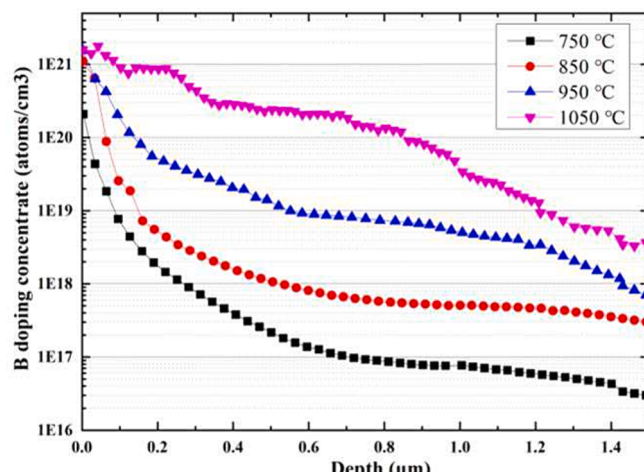


Fig. 12. ECV curves at different temperatures.

Table 1

Electrical I-V parameters of the TOPCon cell.

Cell Group		Eff (%)	Voc (mV)	Jsc(mA/cm ²)	FF (%)	Rs(Ω)
TOPCon+	Av.	24.93	719.1	40.84	84.89	0.00144
	Max	25.17	719.3	41.19	84.95	0.00142
TOPCon	Av.	24.81	719.1	40.79	84.58	0.00148
	Max	24.94	720.4	40.95	84.54	0.00149

100 cells each group from one batch of substrate, Eff deviation is ± 0.1 .

increase in the *FF* of TOPCon cells, reaching up to 0.41 %. This enhancement is primarily attributable to the use of appropriate thermal diffusion conditions and B-doped Si paste to improve the *FF*.

SE structure has been reported to offer advantages such as reduced Auger recombination, decreased contact recombination, and lower contact resistivity [12,18,31,32]. When the B emitter is formed in the solar cell with reduced doping concentration, it results in diminished Auger recombination and improved solar cell characteristics, particularly the short circuit current density (*J_{sc}*) and *FF*. *Voc* is mainly affected by the doping concentration of bulk Si and pn junction(p+/n). However, in this study, the sheet resistivity of p+/n layer is 108.69 Ω/□, which is similar to standard process TOPCon cell(100–120 Ω/□). So the change of *Voc* is relatively small. The SE structure (p++/n) shows a greater impact on contact resistivity in this study, which affects the *J_{sc}* and *FF* more obviously. The improvement in *FF* observed in this study is mainly attributed to the use of screen-printed Si paste and the appropriate thermal diffusion process. These processes enhance the quality of the PN junction, create a uniform and effective B-doped layer on the Si wafer surface, and reduce defects on the PN junction surface. Additionally, this process reduces the series resistance in the PN junction region and minimizes current losses within the solar cell, thus improving the *FF*.

It is important to note that this study has only conducted limited foundational research on B diffusion through molecular dynamics simulation. Further work is needed to develop and refine the theoretical model, optimize the thermal diffusion curve, and adjust the doping concentration of the B emitter. These efforts will contribute to further enhancing the performance of TOPCon cells.

5. Conclusions

In this study, the atomic-level diffusion behavior of B-doped Si was elucidated through molecular dynamics methods. The diffusion characteristics of B in Si, dependent on temperature and time, were successfully identified. The simulation results reveal that only a limited number of B atoms diffuse into Si along the Z direction during the diffusion process. The quantity and depth of B atom diffusion are contingent on temperature and time, with higher temperatures resulting in more B atoms diffusing deeper into the material. The experimental results of thermal diffusion are consistent with the simulation findings. As the temperature increases, the sheet resistance decreases, and with higher doping concentrations, the junction depth increases. Considering the practical challenges and cost implications of the process, one-step B diffusion was carried out using BC₃ and B-doped Si paste as the B source. The thermal diffusion process at 950 °C for 20 min was selected to achieve the desired p+/n and p++/n doping concentrations and connection depths, resulting in an efficient Topcon + cell. The maximum B doping concentrations for the p+ and p++ layers are 8.68×10^{18} atom/cm³ and 2.35×10^{19} atom/cm³, respectively. The connection depths of p+/n and p++/n are 0.53 μm and 0.82 μm, respectively. Ultimately, the I-V performance test demonstrated an efficiency improvement of 0.23 %, primarily attributable to the 0.41 % increase in the *FF*. This method has the potential to optimize the B diffusion curve and serves as a valuable tool for enhancing the conversion efficiency of Si-based solar cells.

CRediT authorship contribution statement

X. Liu contributed to writing-original draft and formal analysis. J. Sun and Y. Huang contributed to investigation. L. Jiang and S. Liu contributed to visualization and validation. F. Qian and H. Shen involved in methodology and formal analysis. Y. Yang and R. Chen involved in resources and writing-review and editing. G. Song contributed to writing-review and editing. J. Hong contributed to conceptualization, funding acquisition and supervision. All authors read and approved the final manuscript.

Declaration of competing interest

The authors declare that they have no known competing financial interests or personal relationships that could have appeared to influence the work reported in this paper.

Acknowledgments

This work was supported by the Natural Science Foundation of China under Grants 51805466 and the 333 High-level Talents Training Project of Jiangsu Province (China) under Grants 153519050.

Appendix A. Supplementary data

Supplementary data to this article can be found online at <https://doi.org/10.1016/j.solener.2024.112448>.

References

- [1] Q. Yang, Z. Liu, Y. Lin, et al., Passivating contact with phosphorus-doped polycrystalline silicon-nitride with an excellent implied open-circuit voltage of 745 mV and its application in 23.88% efficiency TOPCon solar cells [J], Solar RRL 5 (11) (2021).
- [2] S. Ma, B. Liao, F.Y. Qiao, et al., 24.7% industrial tunnel oxide passivated contact solar cells prepared through tube PECVD integrating with plasma-assisted oxygen oxidation and in-situ doped polysilicon [J], Sol. Energy Mater. Sol. Cells 257 (2023).
- [3] M.Q. Khokhar, S.Q. Hussain, S. Chowdhury, et al., High-efficiency hybrid solar cell with a nano-crystalline silicon oxide layer as an electron-selective contact [J], Energ. Convers. Manage. 252 (2022).
- [4] H. Du, Z. Liu, W. Liu, et al., Concurrently preparing front emitter and rear passivating contact via continuous PECVD deposition plus one-step annealing for high-efficiency tunnel oxide passivating contact solar cells [J], Solar RRL 7 (7) (2023).
- [5] Q. Wang, H. Peng, S. Gu, et al., High-efficiency n-TOPCon bifacial solar cells with selective poly-Si based passivating contacts [J], Sol. Energy Mater. Sol. Cells 259 (2023).
- [6] R. Liu, L. Yin, Y. Zhou, An improved process for bifacial n-PERT solar cells fabricated with phosphorus activation and boron diffusion in one-step high temperature [J], Journal Wuhan University of Technology, Materials Science Edition 37 (6) (2022) 1056–1060.
- [7] B. Yu, R. Wang, J. Shi, et al., Impact of boron doping concentration on tunnel oxide passivated contact in front surface for N-type poly-si based passivated contact bifacial solar cells [J], IEEE J. Photovoltaics 12 (3) (2022) 669–677.
- [8] M. Mesmer, S. Bashardoust, U. Belledin, et al. High Throughput Boron emitter formation from pre-deposited APCVD BSG layers for TOPCon solar cells; proceedings of the 49th IEEE Photovoltaics Specialists Conference, PVSC 2022, June 5, 2022 - June 10, 2022, Philadelphia, PA, United states, F, 2022 [C]. Institute of Electrical and Electronics Engineers Inc.
- [9] Y. Li, H. Shen, Z. Hou, et al., Formation of emitter by boron spin-on doping from SiO₂ nanosphere and properties of the related n-PERT solar cells [J], Sol. Energy 225 (2021) 317–322.
- [10] F. Feldmann, M. Bivour, C. Reichel, et al., Passivated rear contacts for high-efficiency n-type Si solar cells providing high interface passivation quality and excellent transport characteristics [J], Sol. Energy Mater. Sol. Cells 120 (2014) 270–274.
- [11] M. Li, J. Wong, et al., Predictive simulation framework for boron diffused p+ layer optimization: sensitivity analysis of boron tube diffusion process parameters of industrial n-type silicon wafer solar cells [J], Sol. Energy Mater. Sol. Cells 189 (2019) 63–74.
- [12] J. Hong, X. Liu, J.W. Ge, et al., Superb improvement of boron doping in selective emitter for TOPCon solar cells via boron-doped silicon paste [J], Sol. Energy 247 (2022) 115–122.
- [13] S. Babak, J. Thomas, Lenosky, et al., Mechanism of boron diffusion in silicon: an ab initio and kinetic Monte Carlo study [J], Phys. Rev. Lett. 83 (21) (1999) 4341–4344.

- [14] I. Kurachi, K. Yoshioka, Enhancement and retardation of thermal boron diffusion in silicon from atmospheric pressure chemical vapor deposited boron silicate glass film [J], *Jpn. J. Appl. Phys.* 53 (3) (2014).
- [15] G. Zhu, J. Sun, L. Zhang, et al., Molecular dynamics simulation of temperature effects on deposition of Cu film on Si by magnetron sputtering [J], *J. Cryst. Growth* 492 (2018) 60–66.
- [16] Q. Wang, K. Guo, L. Yuan, et al., Boron tube diffusion process parameters for high-efficiency n-TOPCon solar cells with selective boron emitters [J], *Sol. Energy Mater. Sol. Cells* 253 (2023).
- [17] H. Cheng, W. Liu, Z. Liu, et al., Emitter formation with boron diffusion from PECVD deposited boron-doped silicon oxide for high-efficiency TOPCon solar cells [J], *Sol. Energy Mater. Sol. Cells* 240 (2022).
- [18] X. Li, Q. Wang, X. Dong, et al., Optimization of efficiency enhancement of TOPCon cells with boron selective emitter [J], *Sol. Energy Mater. Sol. Cells* 263 (2023).
- [19] L. Wang, B. Shen, F. Sun, Investigation of the atomic-scale friction of boron doped diamond using molecular dynamics [J], *J. Comput. Theor. Nanosci.* 11 (6) (2014) 1550–1555.
- [20] C. Liu, E. Jin, S. He, et al., Molecular dynamics study on doping defected graphene by boron [J], *Fullerenes, Nanotubes, Carbon Nanostruct.* 24 (6) (2016) 363–370.
- [21] M. Omidi, Z. Karimi, S. Rahmani, et al., Molecular dynamic study of perovskite with improved thermal and mechanical stability for solar cells application: calculation the final strength of the modeled atomic structures and the young's modulus [J], *Eng. Anal. Bound. Elem.* 156 (2023) 1–7.
- [22] S.D.V.S.S.V. Siruvuri, P.R. Budarapu, M. Paggi, Influence of cracks on fracture strength and electric power losses in silicon solar cells at high temperatures: deep machine learning and molecular dynamics approach [J], *Appl. Phys. A Mater. Sci. Process.* 129 (6) (2023).
- [23] J. Tersoff, Empirical interatomic potential for silicon with improved elastic properties [J], *Phys. Rev. B Condens. Matter* 38 (14) (1988) 9902–9905.
- [24] C.M. Marian, M. Gastreich, A systematic theoretical study of molecular Si/N, B/N, and Si/B/N(H) compounds and parameterisation of a force-field for molecules and solids [J], *Molecular Structure (theochem)* 506 (2006) 107–129.
- [25] J. Hong, R. Xuan, H. Huang, et al., B-doped nano-Si-paste by picosecond laser cladding [J], *Zhongguo Jiguang/Chinese Journal of Lasers* 43 (9) (2016).
- [26] J. Hong, R. Xuan, H. Huang, et al., Si paste technology for high-efficiency solar cells [J], *Sol. Energy* 135 (2016) 70–76.
- [27] T. Oku, M. Kanayama, Y. Ono, et al., Microstructures, optical and photoelectric conversion properties of spherical silicon solar cells with anti-reflection SnO_x: F thin films [J], *Jpn. J. Appl. Phys.* 53 (5S1) (2014).
- [28] J.L. Bryan, J.V. Carpenter, Z.J. Yu, et al., Aluminum–silicon interdiffusion in silicon heterojunction solar cells with a-si:H(i)/a-si:H(n/p)/Al rear contacts. [J], *J Phys D Appl Phys* 54 (2021) 134002.
- [29] W. Lin, C. Daming, C. Liu, et al., Green-laser-doped selective emitters with separate BBr₃ diffusion processes for high-efficiency n-type silicon solar cells [J], *Sol. Energy Mater. Sol. Cells* 210 (2020).
- [30] P. Padhammath, N. Nampalli, A. Khanna, et al., Progress with passivation and screen-printed metallization of boron-doped monoPoly™ layers [J], *Sol. Energy* 231 (2022) 8–26.
- [31] S. Jeong, Y. Cha, S. Kim, et al., Analysis of selective emitter formation technology of n-TOPCon solar cell [J], *Trans. Korean Inst. Electr. Eng.* 71 (2022) 114–120.
- [32] D. Ding, Z. Du, R. Liu, et al., Laser doping selective emitter with thin borosilicate glass layer for n-type TOPCon c-Si solar cells [J], *Sol. Energy Mater. Sol. Cells* 253 (2023).